J Therm Spray Tech (2019) 28:1739–1748
https://doi.org/10.1007/s11666-019-00915-8

PEER REVIEWED

Enhanced Electrochemical and Tribological Properties of AZ91D Magnesium Alloy via Cold Spraying of Aluminum Alloy

Sumera Siddique[1,2] · Cheng-Xin Li[3] · Ayrton A. Bernussi[2,4] · Syed Wilayat Hussain[5] · Muhammad Yasir[5]

Submitted: 27 December 2018 / in revised form: 12 July 2019 / Published online: 20 September 2019

Abstract Magnesium (Mg) alloys have remarkable physical and mechanical properties for various aerospace applications. However, the high corrosion susceptibility and low wear resistance of Mg alloys restrict their wider use. To overcome these problems, 6061 Al alloy coatings were fabricated via the cold spraying process on the AZ91D Mg alloy substrate and a detailed comparative study on the wear and corrosion properties was carried out. The microstructure analysis of the compact coatings revealed low porosity with no phase change during the deposition process. The coatings showed improved corrosion resistance up to seven times as confirmed by potentiodynamic polarization and electrochemical impedance spectroscopy measurements in 3.5 wt.% NaCl aqueous solution. The as-deposited coatings were also compared with commercial bulk alloys of similar composition for their suitability to industrial applications. The tribological behavior of the coatings and substrate was investigated using tribometer. The wear resistance of the coatings improved more than two orders of magnitude as compared to the substrate. Abrasive and oxidative wear mechanisms were dominant in the coatings and substrate. The results showed that cold spraying of 6061 Al alloy on AZ91D Mg alloy could be an auspicious process to overcome the poor corrosion and wear resistance of this Mg alloy for practical industrial applications.

Keywords cold-sprayed coatings · corrosion protection · magnesium alloy · wear resistance

✉ Muhammad Yasir
muhammadyasir85@gmail.com

[1] Department of Physics and Astronomy, Texas Tech University, Lubbock, TX 79409, USA

[2] NanoTech Center, Texas Tech University, Lubbock, TX 79409, USA

[3] State Key Laboratory for Mechanical Behavior of Materials, School of Materials Science and Engineering, Xi'an Jiaotong University, Xi'an 710049, Shaanxi, People's Republic of China

[4] Department of Electrical and Computer Engineering, Texas Tech University, Lubbock, TX 79409, USA

[5] Department of Materials Science and Engineering, Institute of Space Technology (IST), 1-Islamabad Highway, Islamabad 44000, Pakistan

Introduction

Magnesium (Mg) alloys are excellent materials for a large range of applications. Their high damping capacity, low density, good specific strength and recyclability make them an appropriate candidate for the automotive/aerospace applications where these properties have great potential to reduce fuel consumption, thereby contributing to energy savings and reducing environmental impact (Ref 1-4). Although the surface properties of Mg alloys are acceptable for certain applications, their poor corrosion and wear resistance prevent the wider applications of these materials (Ref 5, 6). Therefore, the corrosion protection of Mg alloys has been receiving a great deal of interest in recent years. So far, there are mainly two methodologies to improve the corrosion performance of Mg alloys: composition variation and surface engineering. Pan et al. (Ref 7) reported that the development of new Mg alloys improved their corrosion resistance when compared to commercial Mg alloys. However, their anti-corrosion performance is still poor when compared to Al-based alloys. On the other hand, the surface modification of prevailing Mg alloys is an economical and effective approach to prevent them from

severe corrosion. Protective coatings through different surface treatments such as anodization (Ref 8, 9), chemical vapor deposition (CVD) (Ref 10), spray coatings (Ref 11, 12), chemical conversion (Ref 13-15) and electroplating (Ref 16, 17) have been applied for the surface properties modification of Mg alloys. However, the above-mentioned techniques are restricted either by cost or by performance. In addition, Mg alloys are chemically reactive and their high affinity in aqueous solution makes it challenging to apply these surface modification techniques to these alloys when compared to other metals (Ref 18).

Cold spraying (CS) is a relatively new, simple and innovative coating technique which addresses some shortcomings of the traditional thermal spraying processes (Ref 19-21). In this technique, high-velocity gas stream is used to accelerate powder particles toward the substrate at a temperature much lower than the melting point of the coating material. The impacting solid particles experience plastic deformation and produce a metallurgical bond with the substrate. The low processing temperature prevents various adverse processes such as oxidation, decomposition, evaporation, phase transformation and grain growth of the depositing material (Ref 22, 23). Meanwhile, the high-velocity impacting particles eliminate the interface oxidation and retain the substrate surface fresh which contributes to good particle/substrate adhesion (Ref 24).

The electrochemical studies of Al and its alloys have shown their superior corrosion resistance when compared to Mg and its alloys. This is mainly due to the formation of dense and thin aluminum oxide surface layer (Ref 25, 26). The possibility of getting compact coatings through the cold spraying, good anti-corrosion properties of Al and its alloys make them ideal for corrosion protection metallic coatings. Henao et al. (Ref 27) and Shockley et al. (Ref 28) reported that it is very difficult to coat compact Al or Al alloy coatings using air or nitrogen as accelerating gas in cold spraying. Balani et al. (Ref 29) used helium as the accelerating gas in the cold spraying process to deposit Al alloy coatings. The results confirm that the coatings are compact enough to provide good corrosion resistance. However, the helium gas is much more expensive when compared to nitrogen.

Many studies have been carried out to deposit Al and its alloys composite coatings (Ref 30-32). The blended ceramic particles in pure metal/alloy help to get dense coatings by reducing the inter-particle pores due to the tamping effect of ceramic particles on pre-deposited metallic splats (Ref 32, 33). However, the ceramic particles are brittle in nature and can be easily fractured due to the high impact velocity during the cold spraying process. These crushed ceramic particles may cause crevices and pores in the as-sprayed coating and can provide fast penetrating channels for corrosive media initiating the corrosion process. Cong et al. (Ref 31) showed that the crevices and pores generated in Al + Al_2O_3 composite coatings on steel substrate initiated the corrosion process by the dissolution of the Al matrix localized at the Al_2O_3 particle boundaries. Tao et al. (Ref 34) reported that the cold-sprayed compact pure Al coating on AZ91D alloy show better pitting corrosion resistance than the bulk pure Al in 3.5 wt.% NaCl solution. Hence, a dense and compact coating can provide significant corrosion resistance. Numerous studies have been carried out to study the wear behavior of cold-sprayed Al and its alloys coatings on Mg alloys substrates (Ref 28, 31, 32). The reported results show that the wear rates of the cold-sprayed coatings are several orders of magnitude higher than bulk Al alloys but are several orders of magnitude lower when compared to the substrate material.

6xxx Al alloys are widely used in various applications because of their excellent corrosion resistance and good mechanical properties. The AZ91D Mg alloy has many applications in aerospace/automotive industry. In this study, we selected 6061 Al alloy for surface coating of Mg substrate. Thus, the aim of the work is to deposit a dense Al alloy coating using nitrogen as an accelerating gas via optimization of cold spraying process parameters to enhance the corrosion and wear resistance of the AZ91D Mg substrate. The study of coatings microstructure and the comparison of corrosion and wear mechanisms for the coating and substrate is also the part of the investigation.

Experimental Details

Preparation

The commercially available gas-atomized 6061 Al alloy powder (Xing Rong Yuan Technology Co., Ltd, Beijing, China) was used as the feedstock material for cold spraying with 10-70 μm size range. Particle size and morphology were examined using a field emission scanning electron microscope (FESEM) MIRA3 TESCAN. The secondary electron (SE) image of 6061 Al alloy feedstock powder is shown in Fig. 1(a). Figure 1(b) shows the detailed size distribution of the powder. The particles generally have round morphology, many of these having attached satellite particles.

For the cold spraying, as-cast AZ91D Mg alloy was used as a substrate material. Prior to spraying, the substrate was sandblasted using 24 mesh alumina grits at 0.6 MPa compressed air pressure to improve the coating/substrate adhesion. After sandblasting, the substrate was ultrasonically cleaned in acetone for 10 min. The chemical compositions of the AZ91D Mg alloy substrate, 6061 Al alloy bulk and powder were determined by inductively coupled

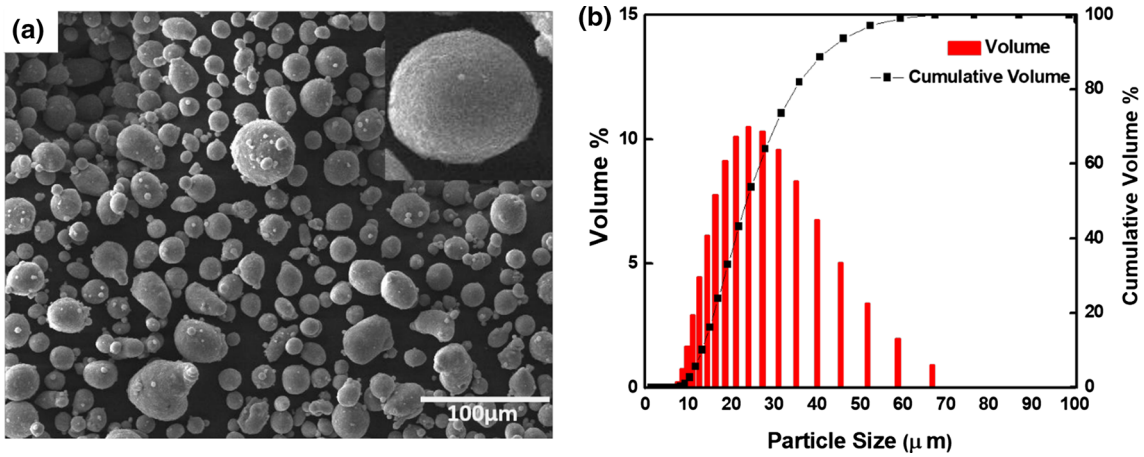

Fig. 1 (a) Morphology; (b) particle size distribution of feedstock 6061 powder

Table 1 Compositions of the AZ91D Mg substrate, 6061 Al alloy bulk and powder as determined by inductively coupled plasma optical emission spectroscopy

Material	Chemical composition, wt.%								
	Mg	Al	Zn	Mn	Si	Cu	Ni	Fe	Cr
AZ91D	Bal	3.81	0.93	0.32	…	…	0.001	0.003	…
6061 bulk	0.92	Bal	0.13	…	0.22	0.28	……	0.21	0.19
6061 powder	1.08	Bal	0.07	…	0.42	…	……	0.77	0.008

plasma optical emission spectroscopy and are listed in Table 1.

A cold spraying system DWCS-2000 (Dewei Automation Company, Xi'an, China) was used to prepare the 6061 Al alloy coatings with the optimization of process parameters as described below. The system has a convergent–divergent de Laval nozzle, and nitrogen was used as an accelerating gas with a driving pressure of 2.8 MPa. The temperature of the mixing chamber, which is close to the temperature of the powder/gas mixture prior to accelerating through the nozzle throat, was 330 °C. The standoff distance was kept at 20 mm from the nozzle exit to the center of the substrate surface. During deposition, the spray gun was manipulated by a robot traversing at a speed of 40 mm/s across the substrate, the powder feeding rate was about 30 g/min and 5-6 passes were performed to get around 1000-μm-thick coating.

Characterization

The coating/substrate interface was examined using FESEM. The cross section of the coated specimen was prepared to metallographic level using the following procedure: The sample was successively ground to finer grades with wet SiC paper, finishing with the 4000 grit paper. Nylon weave cloth with 6 μm diamond paste was used for polishing followed by soft nap cloth and 1 μm diamond paste. This technique was adopted to minimize the coating/substrate interface rounding due to the variance in hardness of the coating and bulk material (Ref 32). Moreover, to observe the inter-particle bonding, the coating/substrate interface was etched in 5 ml HF, 10 ml H_2SO_4 and 85 ml H_2O solution for 10 s and the cross section was imaged using FESEM. The phases present in the feedstock and coating were investigated using x-ray diffraction (XRD) technique (GNR analytical instruments group EXPLORER).

Electrochemical properties of the 6061 Al alloy-coated AZ91D (coating), AZ91D Mg alloy bulk (substrate) and the 6061 Al alloy bulk were comparatively investigated using Reference 600™ potentiostat (Gamry Instruments). The corrosion resistance of the samples was assessed through potentiodynamic polarization. The tests were performed in a three-electrode conventional glass cell using 3.5 wt.% NaCl aqueous solution. The samples (1 cm^2 area), a standard calomel electrode (SCE) and a graphite rod were used as working, reference and auxiliary electrodes, respectively. Prior to individual measurement, the exposed surfaces of all the samples were ground up to 1200 grit and 2-h stabilization period was given to establish a steady-state open-circuit potential (OCP).

To further understand the effect of coating on the corrosion resistance mechanism, electrochemical impedance spectroscopy (EIS) measurements of the coating, substrate and 6061 Al alloy bulk were taken at OCP using a 10 mV (RMS) amplitude AC voltage. The frequency-dependent

impedances were measured from 0.01 Hz to 100 kHz. All the EIS measurements were taken in 3.5 wt.% NaCl aqueous solution.

The dry sliding wear tests on coating and bulk samples were conducted using a ball-on-disk tribometer (MT/60/NI/HT/L, Microtest SA). A 3-mm-diameter steel ball was used as the counter-body. The samples for the tests were polished up to 1 μm finish. A 3 N load and linear speed of 15 cm s^{-1} were used in this experiment. Tests were performed for a distance of 50 m using a 6 mm track diameter. After the wear test, the wear volume loss was obtained from 3D optical measurement system (Keyence VHX-1000C). To study the worn surface morphology and wear mechanism, FESEM analysis of wear tracks were carried out.

Results and Discussions

Microstructure

The microstructure of the coating/substrate interface is displayed in Fig. 2(a). A thick and dense coating was observed with a porosity level of 2-3 vol.% as measured by image analysis software, and FESEM micrograph indicates deformation of 6061 Al alloy powder during the deposition. The substrate is comparatively softer than 6061 Al alloy, so deformation of the substrate may be caused by the impacting particles and particles are penetrated into the substrate. Hence, no pores or cracks were observed at the interface, as shown in Fig. 2(c). Moreover, for the detailed study of inter-particle bonding, polished and etched cross section of the coating was observed using FESEM as shown in Fig. 2(b). Figure 2(d) shows the etched and enlarged cross section exhibited a well-compacted coating with good inter-particle bonding and few pores.

The XRD patterns of initial 6061 feedstock, as-sprayed coating and 6061 Al alloy bulk are shown in Fig. 3. The patterns revealed the standard peaks for pure Al little displaced on 2θ position because of the alloy elements. After cold spraying of 6061 powder, no other phase was observed on the coated specimen besides 6061 Al alloy (matched with card number 01-074-5237). The missing (220) and (311) planes in XRD pattern of 6061 alloy bulk are the effect of rolling texture.

Electrochemical Behavior

OCP Behavior

In order to monitor the corrosion process of the samples, we used the open-circuit potential (OCP) method as a function of time. As shown in Fig. 4(a), the corrosion potentials for 6061 Al alloy bulk and the substrate

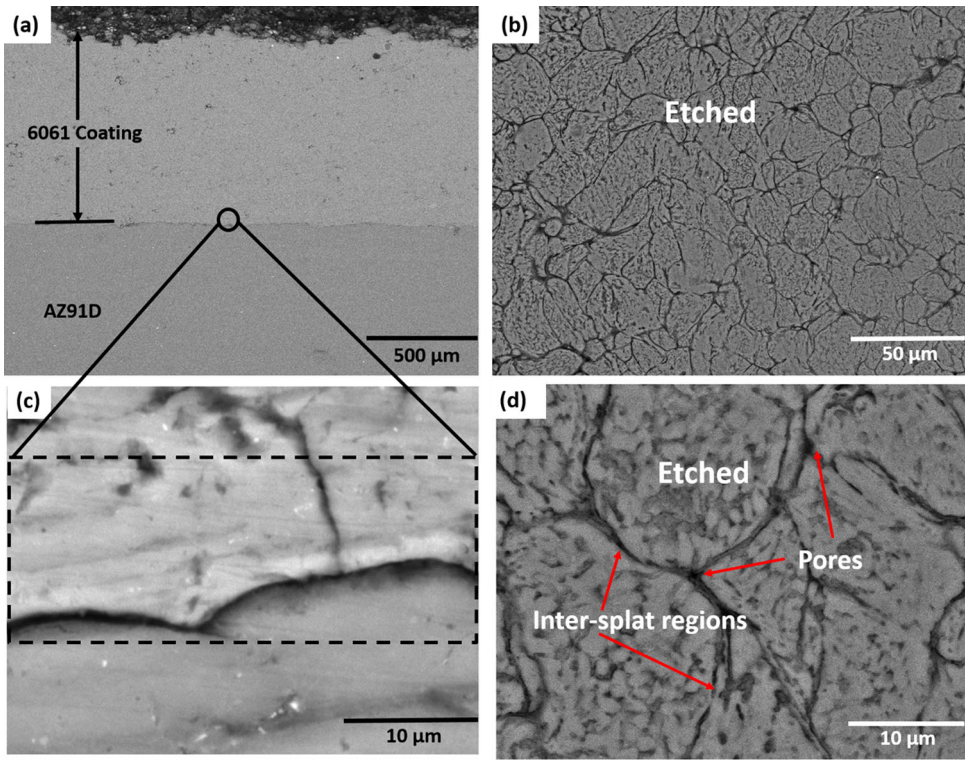

Fig. 2 Field emission scanning electron micrographs: (a) cross-sectional microstructure of cold-sprayed 6061 coating; (b) etched 6061 coating (cross section); (c) a close view of (a) near the coating/substrate interface; (d) enlarged image of (b)

remained stable during the experiment. For the coated sample, the OCP varied from − 1.0 to − 0.9 V over the 3500-s measurement time period, which indicates that hydrous aluminum oxide is produced on the surface. The variation in the OCP amplitude of the coating is higher when compared to the 6061 Al alloy bulk which shows that the dense coating is more active than its bulk alloy and the variation may be due to some reactions at the inter-particle interface. We determined nearly constant OCP values of − 0.73 and − 1.57 V Vs. SCE for 6061 Al alloy bulk and the substrate, respectively, which are comparable to previously reported values (Ref 35, 36). The corrosion potential of the coating moves toward the positive potential because of the higher nobility of the Al in comparison with Mg and hence exhibits improved corrosion resistance than the substrate.

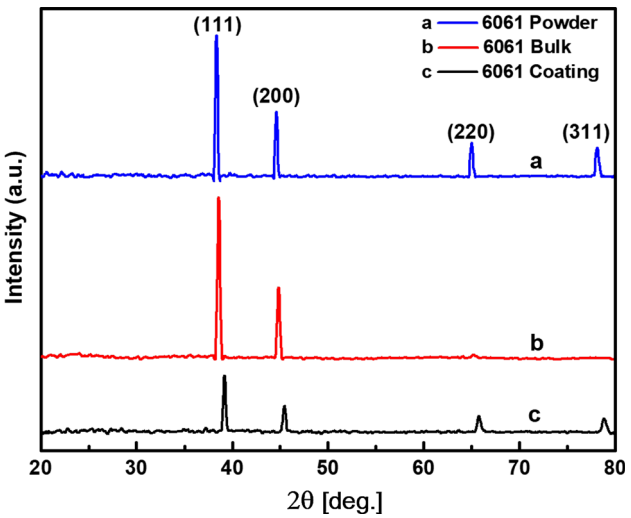

Fig. 3 XRD patterns of the 6061 feedstock powder, coating and bulk

Potentiodynamic Polarization Behavior

Figure 4(b) shows the response of the samples subjected to potentiodynamic polarization testing, curves plotted with a scan rate of 1 mV/s. Corrosion parameters such as the corrosion current density (I_{corr}), corrosion potential (E_{corr}) and corrosion rates were derived from the polarization curves and are summarized in Table 2. The determined values are comparable to those previously reported in the literature (Ref 32, 35-39). Superior stability of the coating when compared to the substrate can be verified from this table. The corrosion current density I_{corr} of the substrate is nearly three times larger than the coating, further confirming the corrosion resistance improvement of the substrate after the coating process. The I_{corr} value of the coating is close to the 6061 Al alloy bulk which indicates that the coating is dense enough to resist the corrosion process like the bulk alloy. The slightly higher value of the I_{corr} for the coating when compared to the 6061 Al alloy bulk is because the coating has numerous inter-particle boundaries, pores and severely deformed microstructure as shown in Fig. 2(d). The anodic polarization curve of the coating exhibits a passive tendency, while that of the 6061 Al alloy bulk shows a rapid increase in current density with the increase in polarization potential (Ref 33). The difference in the behavior is due to the fact that the solution treatment followed by the age hardening of the bulk results in the formation of insoluble intermetallic particles of alloying elements (Al_2Cu, $FeAl_3$ and Mg_2Si) which form local electrochemical cells between them and the aluminum matrix. This gives rise to the localized pitting attack and a coincided pitting corrosion potential (E_{pit}) with the E_{corr}, as shown in Fig. 4(b) (Ref 39). On the other hand, the solid solution of alloying elements makes the coating more active for general corrosion than that of pitting, thus

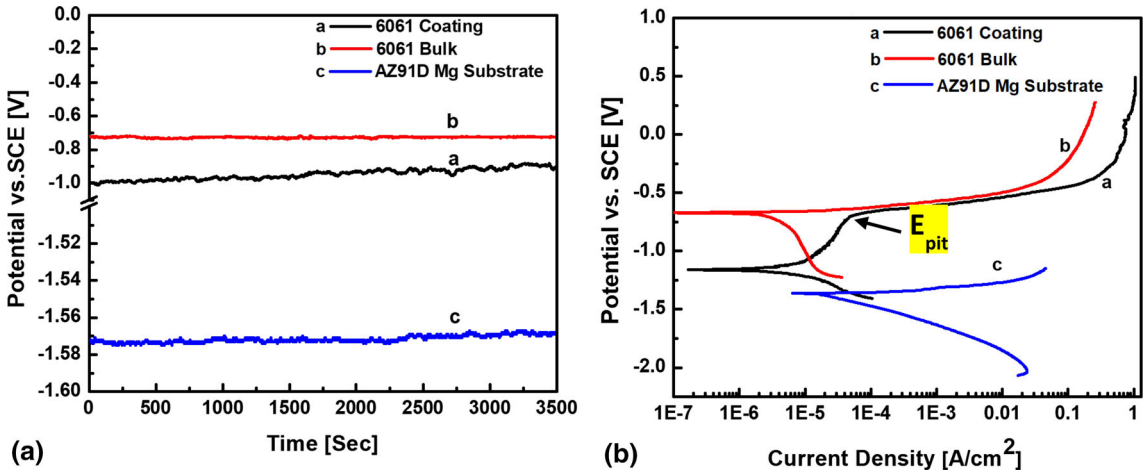

Fig. 4 (a) Open-circuit potential curves; (b) potentiodynamic polarization curves of 6061 coating compared to 6061 bulk and AZ91D Mg substrate in 3.5% NaCl solution

Table 2 Corrosion parameters derived from potentiodynamic curves after 2-h exposure to 3.5% NaCl solution

Alloy	E_{corr}, V	I_{corr}, μA cm^{-2}	Corrosion rate, mpy
6061 coating	− 1.16	7.18	3.11
AZ91D Mg substrate	− 1.37	24.50	20.90
6061 bulk	− 0.67	4.66	2.01

separating the E_{corr} from E_{pit} without changing the E_{pit} (− 0.68 mV) value, as shown in Fig. 4(b). Moreover, a protective $Al(OH)_3$ film is formed on the coating surface in aqueous solution which provides passivation from further corrosion due to its low solubility. Hence, a passivation region can be seen in the polarization curve for the coating. However, the discontinuous hydroxide film (due to the pores and cracks in the coating) causes pitting. The passivation potential of the coating indicates both the beginning of the pitting corrosion potential ($E_{pit.}$) region and the corrosion product's repassivation of the pits (Ref 40, 41).

Electrochemical Impedance Spectroscopy (EIS)

Taking into account the different characteristics of Nyquist and Bode plots shown in Fig. 5(a), (b) and (c), respectively, two equivalent circuits are proposed in the literature to model the frequency-dependent impedance of the investigated samples: one for the 6061 Al alloy coating and bulk as shown in Fig. 5(d) (Ref 35, 38) and the other for the AZ91D Mg alloy substrate as shown in Fig. 5(e). The solution resistance ($R_{s,}$), constant phase element (CPE) and charge transfer resistance (R_{ct}) correspond to the capacitance loop on the higher-frequency side of the Nyquist plot. R_{ct} represents the electron transfer resistance during the electrochemical reaction process. Considering the rough surface of the metal, the constant phase element (CPE) is used instead of the electric double-layer capacitance (Ref 36, 37). The low-frequency loop in Nyquist plots indicates the electrochemical dissolution of passivation film at the outer layer and corresponds to inductance resistance (R_L) and inductance (L). The Nyquist plot of the substrate [inset in Fig. 5(a)] shows one capacitive loop at a high-frequency side and an inductive loop at a low-frequency side. The 6061 Al alloy coating and the bulk both have one capacitance loop with different diameters. This means that both samples have the same corrosion mechanism with different corrosion rates. In addition, the same equivalent circuit well fitted the EIS plots for the 6061 Al alloy coating and the bulk. Moreover, the diameter of the capacitive loop of the coating significantly increased as compared to the substrate which indicates the higher corrosion resistance of the coating compared to the substrate (Ref 37).

Figure 5(b) and (c) shows that for coating the spectrum shows the higher impedance value and broader phase angle when compared to the substrate, which can be attributed to the better protective property of coating compared to the substrate. Moreover, Table 3 shows that there is no significant difference in the solution resistance of all the samples. The value of R_{ct} is usually inversely proportional to the corrosion rate of the sample under investigation. The R_{ct} of the substrate increased from 300 to 6.23 × 10^3 Ω-cm^2 after coating. Thus, R_{ct} value of the substrate increases to several orders of magnitude after coating, but it is little lower than that of the 6061 Al alloy bulk. On the other hand, there is a slight difference in the CPE value for coated and uncoated AZ91D Mg alloy. The higher CPE value for coating as compared to the substrate is because of the porosity and defects in the film (Ref 36, 37). Since this difference is small, the high quality of the coating is confirmed. It can be clearly observed that the coating developed in this work is dense enough and has higher corrosion resistance as compared to the substrate. The corrosion resistance of the coating is also comparable to the 6061 Al alloy bulk.

So far, many studies on the corrosion behavior of Al and its alloys on Mg substrate at different spray conditions have been reported (Ref 32, 35-39). On those reports, it is argued that these coatings are dense enough to provide good protection to Mg-based alloys. It is difficult to rank the results based on I_{corr} values because of the different testing systems and environments. However, in our work, through the series of electrochemical measurement results, it can be concluded that the coatings we fabricated have their corrosion rates comparable to the 6061 Al alloy bulk. Hence, these are dense enough to provide excellent protection to the Mg substrate.

Wear Behavior

An assessment of wear stability of the samples in wear test is the behavior of their coefficient of friction (COF). The COF as a function of distance is shown in Fig. 6(a). The substrate exhibits a higher steady-state COF value of 3.5 as against 0.15 for coating at the beginning of wear test. Then, it rises for the coating to a value of about 0.6. The fluctuating COF behavior can be explained as the dense structure of the coatings is ductile and deforms easily to create a contact between ball and the coating surface resulting in steady-state COF values at the very beginning of the sliding test (Ref 42). Later on, as shown in Fig. 6(c) and (d), the transfer of material from coating to

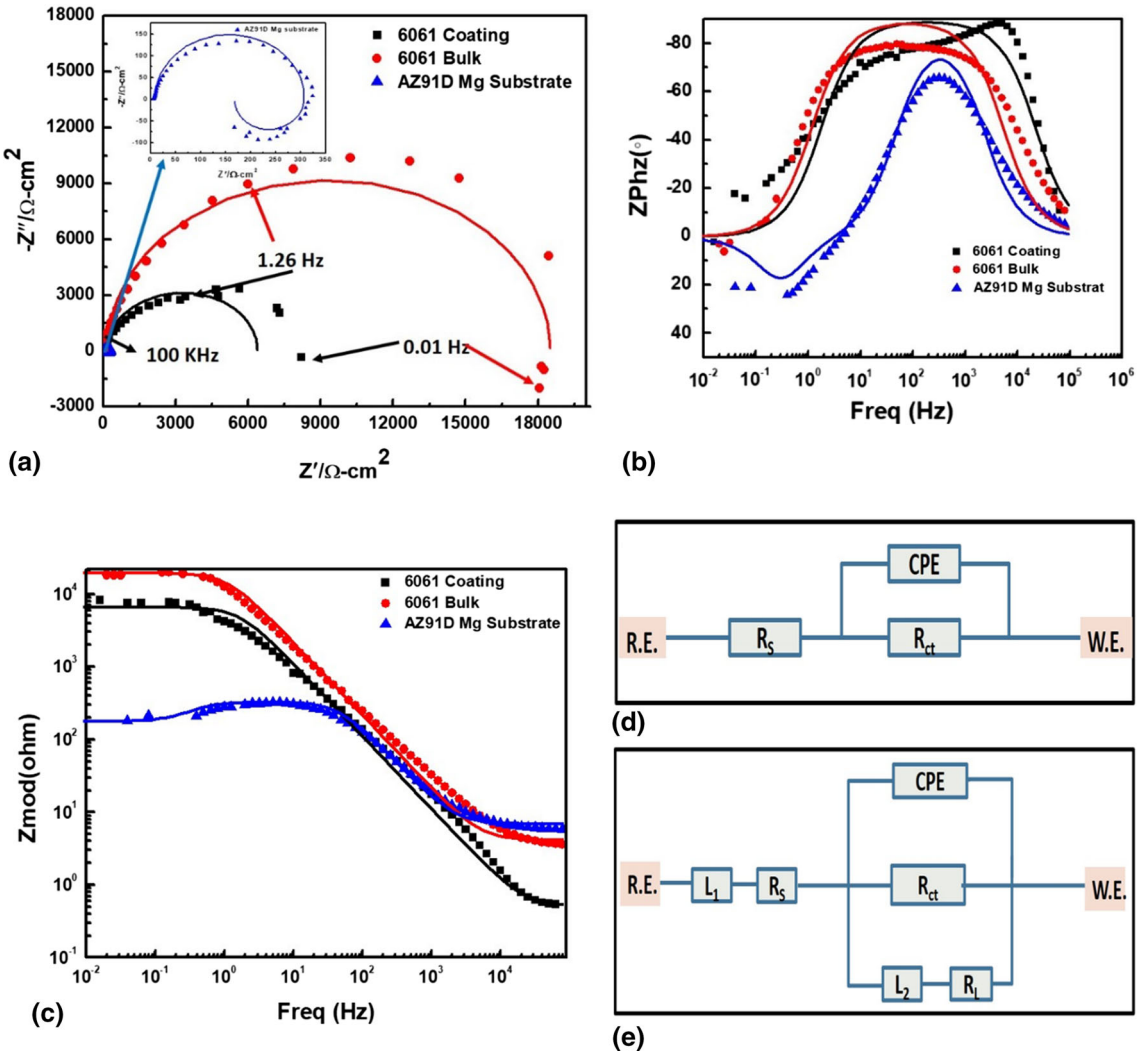

Fig. 5 (a) Nyquist plots; (b, c) Bode plots of 6061 coating, 6061 bulk and AZ91D Mg substrate in 3.5% NaCl solution. Inset in figure (a) is an enlarged Nyquist plot of AZ91D Mg substrate. The solid lines are showing curve fittings. Equivalent circuit for the analysis of the impedance spectra (d) 6061 coating and bulk (e) AZ91D Mg substrate

Table 3 Calculated parameters of the elements of the equivalent electrical circuit for the samples in 3.5 wt.% NaCl solution

Alloy	$L1$, H cm^2	R_{ct}, Ω-cm^2	CPE, μF cm^{-2}	R_s, Ω-cm^2	$L2$, H cm^2	R_L, Ω-cm^2
6061 coating		6.23×10^3	13.86	0.48		
AZ91D Mg substrate	3.62×10^{-12}	300.40	10.28	6.50	233.40	343.40
6061 bulk		18.33×10^3	7.11	3.90		

the steel ball increases the COF which is also evident from the sharp upward deviations in COF values suggesting stick–slip behavior with the periodic material transfer from coating to the steel ball (Ref 32). The fluctuation of COF can be attributed to excessive subsurface fracturing and delamination as well (Ref 43). The 6061 Al alloy bulk has 0.25 steady-state COF value, which is lowest when compared to the substrate and the coating. The coating has lower COF when compared to the substrate, significantly improving the wear resistance of the substrate (Ref 44). Figure 6(b) shows the wear rate comparison for the substrate, 6061 Al alloy bulk and the coating. The 6061 Al alloy exhibits the highest wear resistance. However, it can be seen that the coating has increased the wear resistance of the substrate by several orders of magnitude.

Further, to understand the wear mechanism, worn surfaces of the samples are observed using FESEM imaging. Figure 7(a) shows the circular wear track of the coating,

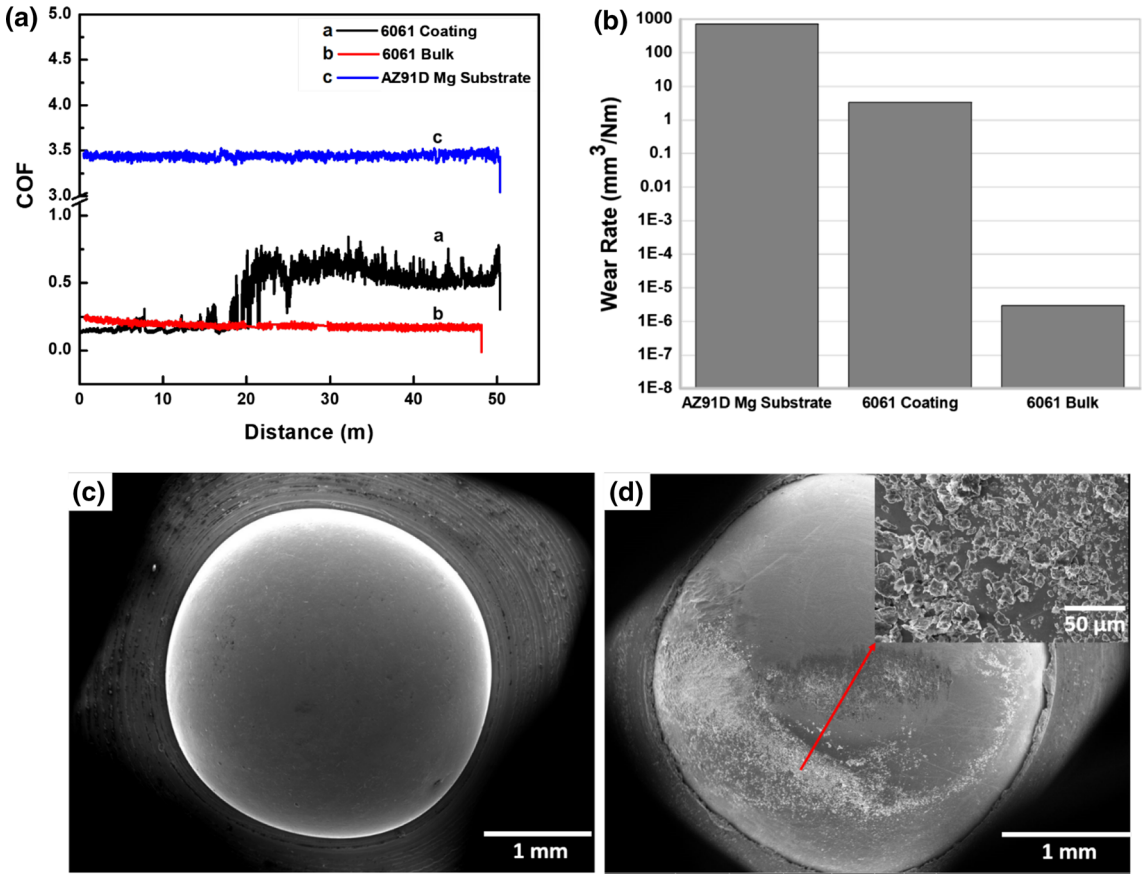

Fig. 6 (a) Coefficient of friction (COF) versus sliding distance and (b) wear rate for 6061 coating, 6061 bulk and AZ91D Mg substrate. Field emission scanning electron micrograph of the steel ball (c) before the wear test and (d) after the wear test. The inset of (d) is the enlarged image of the material stuck to the steel ball after the wear test

and the inset of this figure is the enlarged view of the worn surface. The worn surface has granular appearance, and grains are detached from the surface during the wear test, some of them adhered to the counter-pin and others become wear debris. This is an example of the transfer of material due to adhesion from a softer surface to the harder counter-material and hence adhesive wear (Ref 32). The EDX analysis of the worn surface revealed clear evidence of oxide on the wear track and a typical characteristic of oxidative wear. Figure 7(b) shows the worn surface of the 6061 Al alloy bulk which is a rough surface with mixed regions of micro-abrasive and delamination wear (Ref 43). A wear track for the substrate is shown in Fig. 7(c) which suggest that the surface is worn due to the localized plastic deformation. The furrows are closely spaced, continuous and deep, and the main wear mechanism is abrasive wear (Ref 45, 46).

In this study, the effect of speed and load was not observed, and the selected load is relatively low as we were particularly interested in studying the phenomena involved in the worn surface of the coating rather than making the surface smooth due to the heavy load.

Conclusion

6061 Al alloy coatings were successfully cold-sprayed onto AZ91D Mg alloy substrate for the corrosion and wear resistance enhancement. A dense coating was achieved by the optimization of the cold spraying process parameters. The electrochemical test results reveal that the dense coating has corrosion properties comparable to the 6061 Al alloy bulk in 3.5 wt.% NaCl aqueous solution. Hence, the corrosion resistance of the substrate is enhanced, as evidenced by the corrosion rate of the substrate decreased from 21 to 3 mpy after coating. The low porosity and strong adhesion are the focal aspects resulting in the significant anti-corrosion performance of the coated substrate. Furthermore, the coating has improved the wear resistance of the substrate by several orders of magnitude. Hence, it can be concluded that the 6061 Al alloy cold-sprayed coating developed in this work has significantly enhanced the corrosion and wear properties of Mg substrate and could have promising applications in various industries where low density and high corrosion resistance are required.

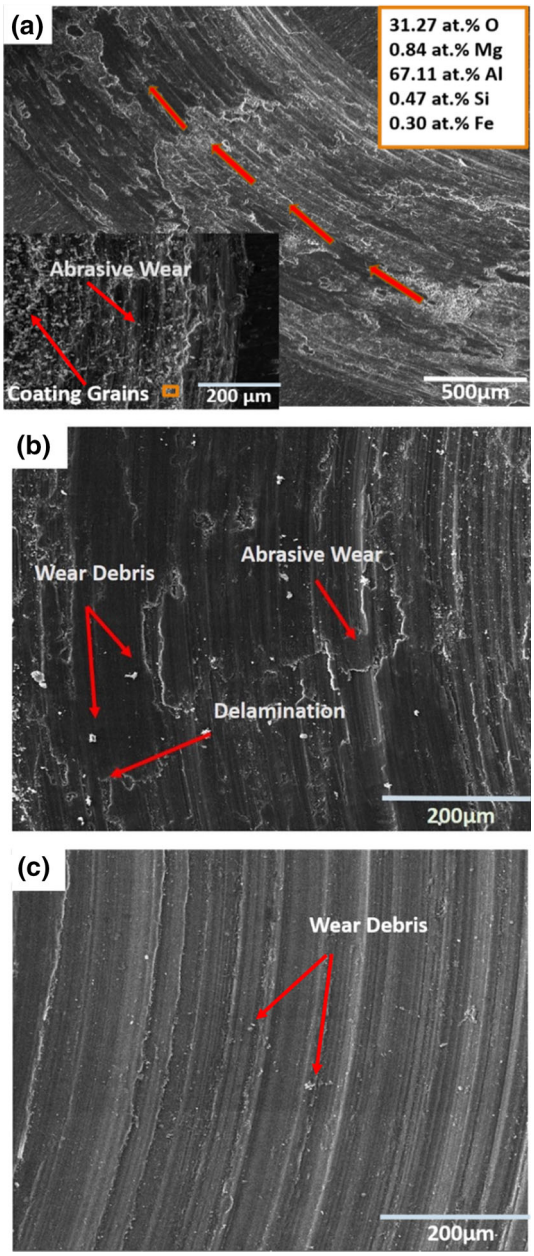

Fig. 7 Field emission scanning electron micrograph of the wear track on (a) 6061 coating inset is enlarge portion of the coating with EDX analysis; (b) 6061 bulk; (c) AZ91D Mg substrate

Acknowledgments This work was financially supported by the Pakistan Science Foundation (PSF/NSFC-II/ENG/C-IST (10)). We are thankful to the thermal spraying laboratory of Xian Jiaotong University for their technical support and help.

References

1. B.L. Mordike and T. Eber, Magnesium Properties Applications Potential, *Mater. Sci. Eng., A*, 2001, **302**, p 37-45
2. H. Furuya, N. Kogiso, S. Matunaga, and K. Senda, Applications of Magnesium Alloys for Aerospace Structure Systems, *Mater. Sci. Forum*, 2000, **350–351**, p 341-348
3. M. Kulekci, Magnesium and Its Alloys Applications in Automotive Industry, *Int. J. Adv. Manuf. Technol.*, 2008, **39**, p 851-865
4. Y. Ali, D. Qiu, B. Jiang, F. Pan, and M. Zhang, Current Research Progress in Grain Refinement of Cast Magnesium Alloys: A Review Article, *J. Alloys Compd.*, 2015, **619**, p 639-651
5. B.A. Shaw and R.C. Wolfe, *Corrosion Resistance of Magnesium alloys, ASM Handbook, Vol 13B, Corrosion: Materials* (ASM International, Materials Park, 2005), pp. 205-227.
6. I.J. Polmear, *Introduction to Magnesium in ASM Specialty Handbook: Magnesium and Magnesium Alloys*, ASM International, Materials Park, 1999, p 3-15
7. F.-S. Pan, M.-B. Yang, and X.-H. Chen, A Review on Casting Magnesium Alloys: Modification of Commercial Alloys and Development of New Alloys, *J. Mater. Sci. Technol.*, 2016, **32**, p 1211-1221
8. T.F. da Conceicao, N. Scharnagl, C. Blawert, W. Dietzel, and K.U. Kainer, Surface Modification of Magnesium Alloy AZ31 by Hydrofluoric Acid Treatment and Its Effect on the Corrosion Behavior, *Thin Solid Films*, 2010, **518**(18), p 5209-5218
9. Y. Mizutani, S.J. Kim, R. Ichino, and M. Okido, Anodizing of Mg Alloys in Alkaline Solutions, *Surf. Coat. Technol.*, 2003, **143**, p 169-170
10. Ch Christoglou, N. Voudouris, G.N. Angelopoulos, M. Pant, and W. Dahl, Deposition of Aluminium on Magnesium by a CVD Process, *Surf. Coat. Technol.*, 2004, **184**, p 149-155
11. H. Pokhmurska, B. Wielage, T. Lampke, T. Grund, M. Student, and N. Chervinska, Post-Treatment of Thermal Spray Coatings on Magnesium, *Surf. Coat. Technol.*, 2008, **202**, p 4515-4524
12. S. Nezamdoust, D. Seifzadeh, and Z. Rajabalizadeh, PTMS/OH-MWCNT Sol–Gel Nanocomposite for Corrosion Protection of Magnesium Alloy, *Surf. Coat. Technol.*, 2018, **35**, p 228-240
13. Y.F. Zhang, C. Blawert, and S.W. Tang, Influence of Surface Pretreatment on the Deposition and Corrosion Properties of Hydrophobic Coatings on a Magnesium Alloy, *Corros. Sci.*, 2016, **112**, p 483-494
14. F.E.T. Heakal, A.M. Fekry, and M.Z. Fatayerji, Influence of Halides on the Dissolution and Passivation Behavior of AZ91D Magnesium Alloy in Aqueous Solutions, *Electrochim. Acta*, 2009, **54**, p 1545–1557
15. L. Liu, F.L. Yuan, and M.C. Zhao, Rare Earth Element Yttrium Modified Mg-Al-Zn alloy: Microstructure, Degradation Properties and Hardness, *Materials*, 2017, **10**, p 477
16. R. Ambat and W. Zhou, Electroless Nickel-Plating on AZ91D Magnesium Alloy: Effect of Substrate Microstructure and Plating Parameters, *Surf. Coat. Technol.*, 2009, **179**(2–3), p 124-134
17. N.E. Mahallawy, Surface Treatment of Magnesium Alloys by Electroless Ni-P Plating Technique with Emphasis on Zinc Pretreatment: a Review, *Key Eng. Mater.*, 2008, **384**, p 241-262
18. J.E. Gray and B. Luan, Protective Coatings on Magnesium and Its alloys. A critical review, *J. Alloys Compd.*, 2002, **336**(1), p 88-113
19. T.V. Steenkiste and J.R. Smith, An Analysis of the Cold Spray Process and Its Coatings, *J. Therm. Spray Technol.*, 2002, **11**(4), p 542-550
20. A. Alkhimov, V. Kosarev, and A. Papyrin, Gas-Dynamic Spraying. An Experimental Study of the Spraying Process, *J. Appl. Mech. Tech. Phys.*, 1998, **39**, p 318-323
21. T. Schmidt, F. Gartner, H. Assadi, and H. Kreye, Development of a Generalized Parameter window for Cold Spray Deposition, *Acta Mater.*, 2006, **54**, p 729-742
22. P. Cavaliere and A. Silvello, Processing Parameters Affecting Cold Spay Coatings Performances, *Int. J. Adv. Manuf. Technol.*, 2014, **71**(1), p 263-277
23. J. Villafuerte, Recent Trends in Cold Spray Technology: Looking at the Future, *Surf. Eng.*, 2010, **26**(6), p 393-394

24. M. Grujicic, J.R. Saylor, D.E. Beasley, W.S. DeRosset, and D. Helfritch, Computational Analysis of the Interfacial Bonding Between Feed-Powder Particles and the Substrate in the Cold-Gas Dynamic-Spray Process, *Appl. Surf. Sci.*, 2003, **219**(3–4), p 211-222
25. C. Vargel, *Corrosion of Aluminum*, Elsevier, Amsterdam, 2004
26. F. Czerwinski, *Magnesium Alloys—Corrosion and Surface Treatments*, InTech, Rijeka, 2011
27. J. Henao, A. Concustell, I.G. Cano, S. Dosta, N. Cinca, J.M. Guilemany, and T. Suhonen, Novel Al-Based Metallic Glass Coatings by Cold Gas Spray, *Mater. Des.*, 2016, **94**, p 253-261
28. J.M. Shockley, S. Descartes, P. Vo, E. Irissou, and R.R. Chromik, The Influence of Al_2O_3 Particle Morphology on the Coating Formation and Dry Sliding Wear Behavior of Cold Sprayed Al-Al_2O_3 Composites, *Surf. Coat. Technol.*, 2015, **270**, p 324-333
29. K. Balani, T. Laha, A. Agarwal, J. Karthikeyan, and N. Munroe, Effect of Carrier Gases on Microstructural and Electrochemical Behavior of Cold-Sprayed 1100 Aluminum Coating, *Surf. Coat. Technol.*, 2005, **195**(2–3), p 272-279
30. H. Bu, M. Yandouzi, C. Lu, D. MacDonald, and B. Jodoin, Cold Spray Blended Al + $Mg_{17}Al_{12}$ Coating for Corrosion Protection of AZ91D Magnesium Alloy, *Surf. Coat. Technol.*, 2012, **207**, p 155-162
31. D. Cong, Z. Li, Q. He, H. Chen, Z. Zhao, L. Zhang, and H. Wu, Wear Behavior of Corroded Al-Al_2O_3 Composite Coatings Prepared by Cold Spray, *Surf. Coat. Technol.*, 2017, **326**, p 247-254
32. K. Spencer, D. Fabijanica, and M. Zhang, The Use of Al-Al_2O_3 Cold Spray Coatings to Improve the Surface Properties of Magnesium Alloys, *Surf. Coat. Technol.*, 2009, **204**, p 336-344
33. Y. Tao, T. Xiong, C. Sun, H. Jin, H. Du, and T. Li, Effect of α-Al_2O_3 on The Properties of Cold Sprayed Al/α-Al_2O_3 Composite Coatings on AZ91D Magnesium Alloy, *Appl. Surf. Sci.*, 2009, **256**, p 261-266
34. Y.-S. Tao, T.-Y. Xiong, C. Sun, L.-Y. Kong, X.-Y. Cui, T.-F. Li, and G.-L. Song, Microstructure and Corrosion Performance of a Cold Sprayed Aluminium Coating On AZ91D Magnesium Alloy, *Corros. Sci.*, 2010, **52**, p 3191-3197
35. M. Shahidi, H. Tajabadipour, H.G. Hakemi, and M.R. Gholamhosseinzadeh, Comparison of Electrochemical Noise Method with the Conventional Electrochemical Techniques for Investigation of the Pitting Corrosion on Al Alloys AA6061 and AA5052 Int, *J. Electrochem. Sci.*, 2013, **8**, p 11734-11751
36. I.B. Singh, M. Singh, and S. Das, A Comparative Corrosion Behavior of Mg, AZ31 and AZ91 Alloys in 3.5% NaCl Solution, *J. Magnes. Alloys*, 2015, **3**, p 142–148
37. S. Zhang, Q. Lia, X. Yangb, X. Zhonga, Y. Daia, and F. Luo, Corrosion Resistance of AZ91D Magnesium Alloy with Electroless Plating Pretreatment and Ni-TiO_2 Composite Coating, *Mater. Charact.*, 2010, **61**, p 269-276
38. C.P.C. Morquecho, C.L. Meléndez, M.I.F. Zamora, R.G.B. Margulis, H.E.E. Ponce, F.A. Calderón, C.G. Tiburcio, and A.M. Villafañe, Electrochemical Impedance Spectroscopy Behavior of Nanometric Al-Cr and Cr-Al Coatings by Magnetron Sputtering, *Int. J. Electrochem. Sci.*, 2012, **7**, p 1125-1133
39. B. Zaid, D. Saidi, A. Benzaid, and S. Hadji, Effects of pH and Chloride Concentration on Pitting Corrosion of AA6061 Aluminum Alloy, *Corros. Sci.*, 2008, **50**, p 1841-1847
40. E. Ghali and R.W. Revie, *Corrosion Resistance of Aluminum and Magnesium Alloys: Understanding, Performance, and Testing*, Wiley, New York, 2010
41. M. Oteyaka, E. Ghali, and R. Tremblay, Corrosion Behaviour of AZ and ZA Magnesium Alloys in Alkaline Chloride Media, *Int. J. Corros.*, 2012, **2012**, p 10
42. S.B. Pitchuka, B. Boesl, C. Zhang, D. Lahiri, A. Nieto, G. Sundararajan, and A. Agarwal, Dry Sliding Wear Behavior of Cold Sprayed Aluminum Amorphous/Nanocrystalline Alloy Coatings, *Surf. Coat. Technol.*, 2014, **238**, p 118-125
43. A.M. Al-Qutub, A. Khalil, N. Saheb, and A.S. Hakeem, Wear and Friction Behavior of Al6061 Alloy Reinforced with Carbon Nanotubes, *Wear*, 2013, **297**, p 752-761
44. Y.-F. Liu, Z.-Y. Xia, J.-M. Han, G.-L. Zhang, and S.-Z. Yang, Microstructure and Wear Behavior of (Cr, Fe)7C3 Reinforced Composite Coating Produced by Plasma Transferred Arc Weld-Surfacing Process, *Surf. Coat. Technol.*, 2006, **201**, p 863-867
45. P.J. Blau and M. Walukas, Sliding Friction and Wear of Magnesium Alloy AZ91D Produced by Two Different Methods. Matthew Walukas, *Tribol. Int.*, 2000, **33**, p 573-579
46. N.N. Aung, W. Zhou, and L.E.N. Lim, Wear Behaviour of AZ91D Alloy at Low Sliding Speeds, *Wear*, 2008, **265**, p 780-786